Ocean Modelling 118 (2017) 118–129

Contents lists available at ScienceDirect

Ocean Modelling

journal homepage: www.elsevier.com/locate/ocemod

Sensitivity of the Antarctic Circumpolar Current transport to surface buoyancy conditions in the North Atlantic

Shantong Sun[a,*], Jinliang Liu[b]

[a] Scripps Institution of Oceanography, University of California San Diego, 9500 Gilman Drive, La Jolla, CA 92093, USA
[b] Department of Oceanography and Coastal Sciences, Louisiana State University, Baton Rouge, LA 70803, USA

ARTICLE INFO

Article history:
Received 21 April 2017
Revised 16 August 2017
Accepted 12 September 2017
Available online 14 September 2017

Keywords:
Antarctic Circumpolar Current
Overturning circulation
North Atlantic

ABSTRACT

The sensitivity of the Antarctic Circumpolar Current (ACC) transport to surface buoyancy conditions in the North Atlantic is investigated using a sector configuration of an ocean general circulation model. We find that the sensitivity of the ACC transport is significantly weaker than previous studies. We attribute this difference to the different depth of the simulated Atlantic Meridional Overturning Circulation. Because a fast restoring buoyancy boundary condition is used that strongly constrains the surface buoyancy structure at the Southern Ocean surface, the ACC transport is determined by the isopycnal slope that is coupled to the overturning circulation in the Southern Ocean. By changing the surface buoyancy in the North Atlantic, the shared buoyancy contour between the North Atlantic and the Southern Ocean is varied, and consequently the strength of the overturning circulation is modified. For different depth of the simulated overturning circulation, the response of the ACC transport to changes in the strength of the overturning circulation varies substantially. This is illustrated in two conceptual models based on the residual-mean theory of overturning circulation. Our results imply that the sensitivity of the ACC transport to surface forcing in the North Atlantic could vary substantially in different models depending on the simulated vertical structure of the overturning circulation.

1. Introduction

The Antarctic Circumpolar Current (ACC) is the world's largest current system. Driven at least partly by the Southern hemisphere westerly wind, the ACC is associated with strongly titled surfaces of constant density, i.e., isopycnals. Through the tilting isopycnals, deep water upwells and ventilates at the Southern Ocean surface (e.g., Marshall and Speer, 2012; Talley, 2013), providing an effective connection between the surface and deep ocean. Consequently, the ACC is uniquely important for global water mass formation (e.g., Talley, 2013; Lamy et al., 2015), air–sea exchanges and redistribution of heat, fresh water, and anthropogenic carbon (e.g., Toggweiler and Russell, 2008; Ito et al., 2010; Tamsitt et al., 2016), and thus for the global climate system.

The ACC is an important part of the global ocean overturning circulation (e.g., Marshall and Speer, 2012; Talley, 2013). In a two-dimensional zonally-integrated view, the global ocean overturning circulation is composed of an upper overturning circulation cell, which is due to the Atlantic Meridional Overturning Circulation (AMOC) and is associated with sinking of the North Atlantic Deep Water (NADW) in the high-latitude North Atlantic, and a lower overturning circulation cell, which is associated with the Antarctic Bottom Water (AABW) formation (Lumpkin and Speer, 2007). Through the ACC, the two overturning circulation cells are coupled to each other, forming a complex three-dimensional structure of the global ocean overturning circulation (Talley, 2013; Ferrari et al., 2014).

In the pycnocline model by Gnanadesikan (1999), the global pycnocline depth and T_{ACC} are linked to processes in the Southern Ocean including surface wind forcing and meso-scale eddies and also to processes outside of the Southern Ocean including deep water formation in the high-latitude North Atlantic and global diapycnal diffusivity. Recent studies using eddy-rich models find that the ACC is largely in an eddy saturated state (e.g., Munday et al., 2013; Bishop et al., 2016), in which additional power input from a stronger wind forcing can be balanced by an intensification of eddies without changing the mean circumpolar flow (Hogg, 2010). Consistent with those eddy-rich simulations, no significant relationship between the ACC transport with changes in the magnitude or position of the wind stress is identified in the Coupled Model Intercomparison Project (CMIP) Phase 5 (e.g., Meijers et al., 2012; Downes and Hogg, 2013). In contrast to the relative insensitivity of T_{ACC} to local processes in the Southern Ocean, the remote ef-

* Corresponding author.
E-mail address: shantong@ucsd.edu (S. Sun).

http://dx.doi.org/10.1016/j.ocemod.2017.09.004
1463-5003/

fects have been suggested to have noticeable influence on the ACC (Munday et al., 2011; Fučkar and Vallis, 2007). Using an ocean general circulation model (OGCM) with an idealized setup, Fučkar and Vallis (2007) found that T_{ACC} varies substantially in response to changes in the surface buoyancy conditions in the North Atlantic, implying a great sensitivity of the T_{ACC} to the NADW formation.

The strong sensitivity of the ACC transport to the NADW formation in Fučkar and Vallis (2007) appears to contradict with some studies using coupled comprehensive climate models (e.g., Wang et al., 2011). By analyzing multiple model simulations from the CMIP 3, which predict consistent weakening of the AMOC in response to anthropogenic activities in the 21st century, Wang et al. (2011) concluded that changes in the AMOC have very minor influence on the ACC transport. The conclusion of Wang et al. (2011) is consistent with some recent studies that emphasize the critical role played by the Southern Ocean processes in determining the global deep ocean stratification (Nikurashin and Vallis, 2011; Wolfe and Cessi, 2010; Sun et al., 2016) and global ocean overturning circulation (Ferrari et al., 2014). However, the complexity of the comprehensive climate models makes it hard to compare directly with Fučkar and Vallis (2007). In particular, the intensification and poleward shift of the westerly wind over the Southern Ocean in Wang et al. (2011) might have counteracted the influence of the AMOC on the ACC transport.

In this study, we revisit the influence of the North Atlantic surface buoyancy conditions on the ACC transport using an OGCM in an idealized configuration. A series of numerical simulations are performed. Two conceptual models are used to interpret the simulation results. We find that the sensitivity of the ACC transport to North Atlantic surface buoyancy conditions strongly depends on the simulated vertical structure of the AMOC.

2. Model and results

2.1. Model setup

We employ the Massachusetts Institute of Technology General Circulation Model (MITgcm; Marshall et al., 1997) to integrate the hydrostatic primitive equations. The model has a flat-bottom rectangular geometry with a reentrant channel to the south (Fig. 1(a)). The semi-enclosed basin represents an idealized Atlantic Ocean, and the reentrant channel represents the Southern Ocean. The model has 25 vertical levels, of which the thickness ranges from 10 m at the surface to 250 m at the ocean bottom. The domain is 2800 m deep, 3200 km wide in the zonal direction, and 8000 km long in the meridional direction. This is half as deep, half as wide, and half as long as the Atlantic in the real ocean in order to perform sufficient amount of simulations on limited computing resources. A submarine sill of 2060 m depth is placed in the reentrant channel to represent the Drake passage. This submarine sill also provides the bottom form stress that balances the momentum input into the ACC from surface wind forcing (Munk and Palmén, 1951). Consistent with the Cartesian grid, a beta plane is adopted and the Coriolis parameter varies linearly in the meridional direction, i.e., $f(y) = f_0 + \beta y$, with $f_0 = -8 \times 10^{-5}\,\mathrm{s}^{-1}$, $\beta = 2.0 \times 10^{-11}\,\mathrm{m}^{-1}\,\mathrm{s}^{-1}$, and y is a Cartesian coordinate that corresponds to latitude.

The horizontal resolution of the model is 80 km. The unresolved mesoscale eddies are represented by the advective form of the Gent and McWilliams (GM) parameterization (Gent and Mcwilliams, 1990) and Redi isopycnal mixing (Redi, 1982) with equal mixing coefficient $K_{GM} = 488\,\mathrm{m}^2/\mathrm{s}$ following Wolfe and Cessi (2011). The GM parameterization is implemented using the boundary-value problem scheme of Ferrari et al. (2010) that parameterizes the diabatic component of eddy flux at the surface layer of ocean where eddy motions become horizontal. The diabatic eddy flux in the surface mixed layer is ignored in Fučkar and Vallis (2007), and this has been suggested by Wolfe and Cessi (2010) to lead to a large residual-mean flow in the Southern Ocean.

The density of seawater is linearly dependent on temperature with a constant thermal expansion coefficient $2.0 \times 10^{-4}\,\mathrm{K}^{-1}$. The seawater salinity is kept at 35 g/kg. We adopt a constant background vertical diffusivity of $2 \times 10^{-5}\,\mathrm{m}^2/\mathrm{s}$ to diffuse the temperature vertically. This small vertical diffusivity is used because we are focusing on the upper overturning circulation cell, which is located above the bottom topography and can be considered to be approximately adiabatic (e.g., Wolfe and Cessi, 2011). The lower overturning circulation, which is associated with the export of AABW, is not well-resolved in this model. The momentum is dissipated via Laplacian viscosity, biharmonic viscosity, vertical viscosity, and bottom drag with coefficients $A_h = 1.0 \times 10^4\,\mathrm{m}^2/\mathrm{s}$, $A_4 = 5.0 \times 10^{12}\,\mathrm{m}^2/\mathrm{s}$, $A_v = 3.0 \times 10^{-3}\,\mathrm{m}^2/\mathrm{s}$, and $r = 4.1 \times 10^{-6}\,\mathrm{s}^{-1}$, respectively. Convection is handled by the K-Profile Parameterization (KPP) scheme (Large et al., 1994). Therefore, the actual vertical diffusivity and viscosity can be different from the background value depending on the state of hydrostatic stability.

The wind stress forcing is symmetric with respect to the equator ($y = 4000$ km) and is uniform in the zonal direction (Fig. 1(b)). The surface temperature is relaxed to a profile ($T_s(y)$) that is expressed as

$$T_s(y) = T_0(y) + \delta_T \mathrm{e}^{-20(y/L_y-1)^2}, \tag{1}$$

where $T_0(y)$ is the symmetric reference temperature profile and is given in Fig. 1(c), L_y is the meridional width of the basin, and δ_T controls how much warmer the surface ocean in the North Atlantic is than the Southern Ocean. The relaxation time scale is 10 days and is close to that concluded by Haney (1971) from observations. Because of this fast-restoring boundary condition, the surface density is essentially specified in the Southern Ocean (see Figs. 1(c) and2) and the ACC transport is determined by the isopycnal slope, which is coupled to the overturning circulation based on the residual-mean theory in Marshall and Radko (2003). Previous studies have shown that the AMOC strength scales linearly with the shared surface density range between the Southern Ocean and the North Atlantic (Nikurashin and Vallis, 2012; Wolfe and Cessi, 2011). Therefore, by changing the surface density in the North Atlantic and keeping the surface density largely unchanged in the Southern Ocean, the strength of the AMOC is varied. Throughout this study except for Section 4, we have kept the other processes unchanged, including surface wind forcing, eddy diffusivity, and diapycnal diffusivity.

Accordingly, δ_T determines the shared density range between the Southern Ocean and the North Atlantic, and consequently it controls the intensity of the AMOC (Wolfe and Cessi, 2011; Nikurashin and Vallis, 2012). At $\delta_T = 0\,^\circ\mathrm{C}$, the temperature forcing is symmetric with respect to the equator. By increasing δ_T, the shared density between the Southern Ocean and the North Atlantic is reduced such that the AMOC is weakened (see Fig. 2, Wolfe and Cessi, 2011; Nikurashin and Vallis, 2012), along with a slight increase in the lower overturning circulation cell due to the contraction of the upper cell (cf. Jansen and Nadeau, 2016). Beyond $\delta_T \approx 5\,^\circ\mathrm{C}$, there is no shared density between the North Atlantic and the Southern Ocean, and the pole-to-pole overturning circulation disappears.

2.2. Simulation results

A series of simulations are performed to test the sensitivity of T_{ACC} to the surface buoyancy condition in the North Atlantic, which is achieved by varying δ_T systematically. Each simulation is initiated from a motionless state and is run for over 3500 years until

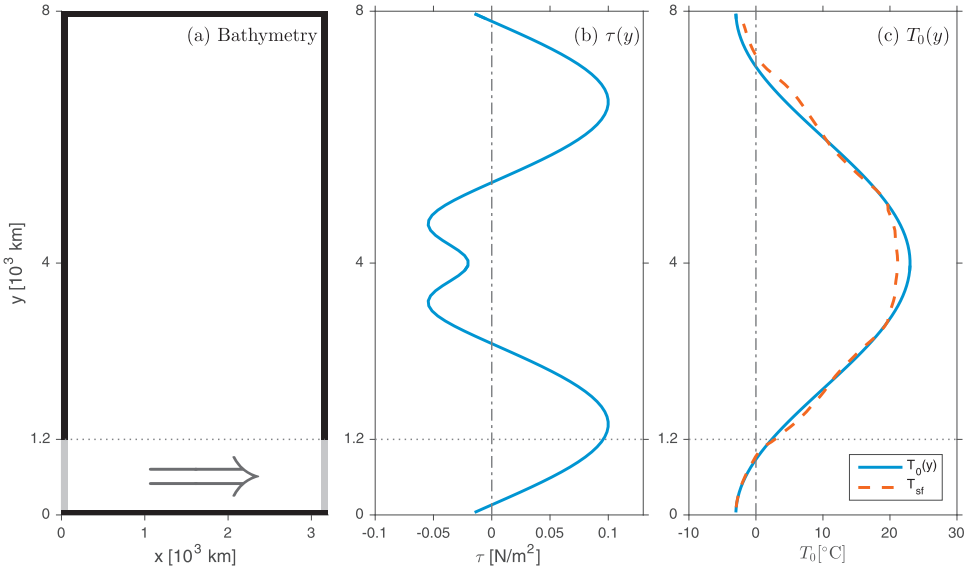

Fig. 1. (a) Bathymetry of the basin. The black thick line indicates the idealized continents. The gray thick line indicates the submarine sill that represents the Drake passage. The gray arrow indicates the direction of the ACC. (b) Surface wind stress forcing ($\tau(y)$) which is symmetric about the equator ($y = 4000$ km) in the meridional and uniform in the zonal direction. (c) Profile of the symmetric reference temperature ($T_0(y)$; blue solid line) in Eq. (1). The zonal-mean surface temperature at $\delta_T = 0.5$°C (T_{sf}) is plotted as red dashed line for comparison. The northern boundary of the reentrant channel is plotted in each panel as gray dotted lines. The zero position of τ and T are plotted in panels (b) and (c) as gray dash–dotted lines. (For interpretation of the references to color in this figure legend, the reader is referred to the web version of this article.)

approximate equilibrium, at which the linear trend of T_{ACC} over the last 100 years is less than 1 Sv/century (1 Sv=10^6 m^3/s). The last 50 years of each simulation is used for the following analysis.

The residual-mean overturning circulation streamfunction is defined as:

$$\psi(y,\theta) = \frac{1}{t_0}\int_0^{t_0}\int_0^{L_x}\int_{-H}^{\zeta(x,y,\theta,t)} v_r\, dz\, dx\, dt, \tag{2}$$

where x and z are Cartesian coordinates that correspond to longitude and depth, t is time, H is the depth of the basin, L_x is the zonal width of the basin, $t_0 = 50$ years, θ is potential temperature, $\zeta(x, y, \theta, t)$ represents the height of isotherms θ, and v_r is the residual velocity that includes both Eulerian-mean velocity and eddy bolus velocity due to the GM parameterization. Fig. 2 shows two examples of the residual-mean overturning circulation streamfunction that are remapped to height coordinate using the zonal-mean time-mean depth of each isotherm

$$\overline{\zeta}(y,\theta) = \frac{1}{t_0}\int_0^{t_0}\frac{1}{L_x}\int_0^{L_x}\zeta(x,y,\theta,t)dz\,dx\,dt, \tag{3}$$

for $\delta_T = 1$°C and $\delta_T = 4$°C, respectively. The clockwise pole-to-pole overturning circulation is an idealized representation of the AMOC. It is substantially reduced at $\delta_T = 4$°C compared to $\delta_T = 1$°C as expected. The lower overturning circulation cell is not well resolved because of the low diapycnal diffusivity used in our model.

The intensity of the pole-to-pole overturning circulation (ψ_i) is defined as the maximum streamfunction that connects the Southern Ocean and the North Atlantic, i.e., the minimum of the maximum streamfunction at each latitude below the surface wind-driven gyre:

$$\psi_i = \min\{\max\{\psi(y,\theta < 3°\text{C}),\theta\}, y\} \quad \text{for } 1200\,\text{km} < y < 7000\,\text{km}, \tag{4}$$

where the operator $\max\{f(\mu_1, \mu_2), \mu_2\}$ and $\min\{f(\mu_1, \mu_2), \mu_2\}$ represent the maximum and minimum of the function $f(\mu_1, \mu_2)$ with respect to the dimension μ_2 for a constant μ_1. This is defined for $\theta < 3$°C in order to exclude the wind-driven gyre circulation. Because the isopycnal slope is more relevant to local overturning circulation as discussed in Section 3, we also define the intensity of the Southern Ocean residual-mean overturning circulation (ψ_s) as

$$\psi_s = \max\{\psi(L_s,\theta)\}, \tag{5}$$

where $L_s = 1200$ km represents the northern boundary of the reentrant Southern Ocean. Variations of ψ_i and ψ_s with respect to δ_T are given in Fig. 3(a). At $\delta_T = 5$ °C, ψ_s is reduced to around 1.2 Sv although the pole-to-pole overturning circulation disappears as the shared density range between the North Atlantic and the Southern Ocean is reduced to zero. The difference between the locally defined ψ_s and the pole-to-pole overturning circulation is due to a local clockwise overturning circulation between $y = 1200$ km and $y = 2000$ km (Fig. 2). This local overturning circulation is a remanent of the wind-driven overturning circulation (sometimes called "Deacon cell"). It is likely due to the constant eddy thickness diffusivity adopted in our model, which might underestimate the effect of eddies in compensating the wind-driven overturning circulation (cf. Gent and Danabasoglu, 2011; Gent, 2016).

The circumpolar transport of the ACC with respect to changes in ψ_s is plotted in Fig. 3(b). From $\delta_T = 0.5$ °C to $\delta_T = 5.0$ °C, ψ_s decreases from 2.6 Sv to 1.2 Sv and T_{ACC} increases from 62 Sv to 76 Sv. In comparison, T_{ACC} increases from 25 Sv to 125 Sv in Fučkar and Vallis (2007, their Fig. 3) for a similar change of the temperature forcing. To exclude the possibly geometrical influence due to the different size of model domain, we will normalize the ACC transport in the following discussions with a reference ACC transport (see details below).

Wolfe and Cessi (2010) attributed the large sensitivity of T_{ACC} observed in Fučkar and Vallis (2007) to their strong residual-mean overturning circulation in the Southern Ocean. However, the magnitude of the residual-mean overturning circulation in our simulation (see Fig. 3(a)) is actually close to or even larger than Fučkar and Vallis (2007, their Fig. 2). Therefore, the strong sensitivity of T_{ACC} to the North Atlantic surface forcing in Fučkar and Vallis (2007) cannot be explained by the magnitude of the residual-mean overturning circulation in the Southern Ocean. As seen in Fig. 2, the clockwise pole-to-pole overturning circulation is limited to the upper 1 km in both cases of Fig. 2. In comparison, the

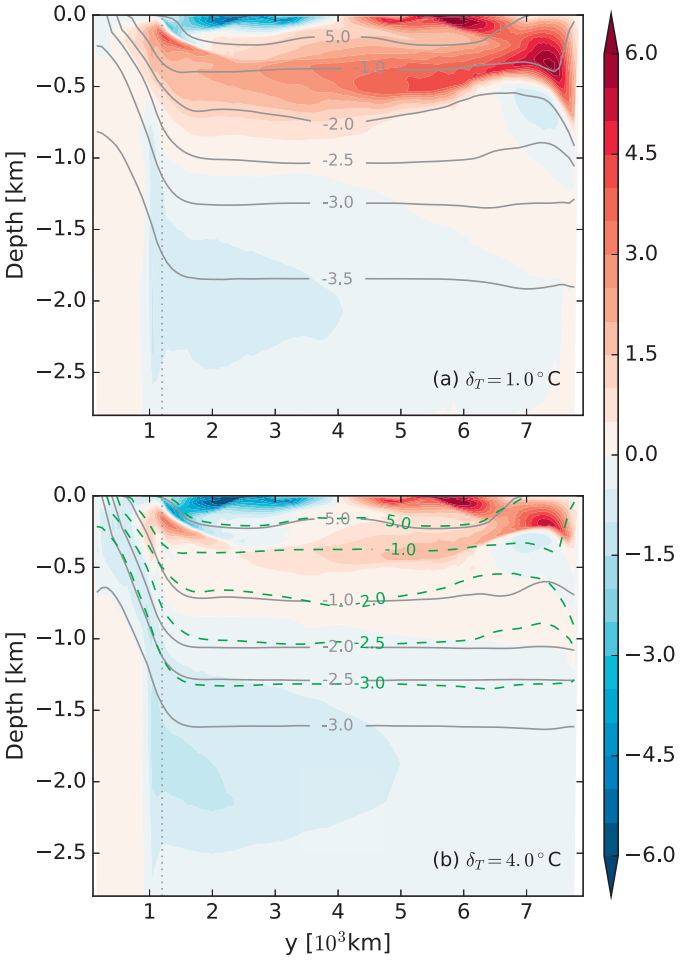

Fig. 2. Residual-mean overturning circulation streamfunction (color shading) $\psi(y, \theta)$ remapped to height coordinate at $\delta_T = 1\,^\circ$C (a) and $\delta_T = 4\,^\circ$C (b), plotted in units of Sv. The gray solid lines represent the mean depth of isotherms that is defined by Eq. (3) and labeled in unit of °C. Five isotherms from panel (a) are plotted in panel (b) as green dashed lines to show the change of isopycnal slope. The northern boundary of the reentrant Southern Ocean is plotted as gray dotted lines. (For interpretation of the references to color in this figure legend, the reader is referred to the web version of this article.)

AMOC in Fučkar and Vallis (2007) reaches around 2500 m in their symmetric forcing case (corresponding to $\delta_T = 0\,^\circ$C in our study) and then shoals upward substantially to a shallower depth as the surface temperature increases in the North Atlantic (their Fig. 2). Therefore, the different sensitivity of the ACC transport is likely related to the different vertical structure of the overturning circulation as explained in the next section using conceptual models.

3. Conceptual models

In this section, we develop a 2.5-layer conceptual model and a continuously stratified conceptual model of the Southern Ocean circulation based on the residual-mean theory of Marshall and Radko (2003) in order to understand the influence of the overturning circulation structure on the ACC transport. The 2.5-layer conceptual model can be considered to be a generalization of the pycnocline model of Gnanadesikan (1999). A similar multi-layer generalization of Gnanadesikan (1999) is developed for the Atlantic basin by Marshall and Zanna (2014). Different from Marshall and Radko (2003), in which the overturning circulation is part of the solution, we specify the overturning circulation streamfunction as an input for our conceptual model in order to discuss the response of the ACC transport to variations in the overturning circulation. In the conceptual models of this section, we use a shifted coordinate ($y_s = y - L_s$) for analytical convenience. The subscript for y_s is dropped in the discussion hereafter for notation conciseness, i.e., the origin of the y axis is at the northern boundary of the Southern Ocean in this section.

3.1. 2.5-layer conceptual model

In this section, a 2.5-layer conceptual model is developed that includes two active layers (ρ_1 and ρ_2) and a motionless abyssal layer (ρ_3) as shown in the schematic Fig. 4. The three layers, which are separated by two pycnoclines, respectively, represent intermediate water, deep water, and bottom water from top to bottom. The stratification across the two pycnoclines is, respectively, noted as g_1' and g_2', where $g_1' = g(\rho_2 - \rho_1)/\rho_0$, $g_2' = g(\rho_3 - \rho_2)/\rho_0$, and ρ_0 is the reference density. The two active layers outcrop through the surface mixed layer in the Southern Ocean. For simplicity, we keep the outcropping position of the two pycnoclines $y = -L_1$ and $y = -L_2$ unchanged, i.e., we assume L_1 and L_2 to be constant. In the continuously stratified model, we will relax the assumption of constant L_1 and L_2.

The AMOC is carried by the top two layers. Following Marshall and Radko (2003), we define the residual-mean overturning circulation streamfunction for our layer model as

$$\psi_1 = \int_0^{L_x}\int_{-h_1}^{0} v\,dzdx = \psi_1^+ + \psi_1^*, \tag{6}$$

$$\text{and} \quad \psi_2 = \int_0^{L_x}\int_{-h_2}^{0} v\,dzdx = \psi_2^+ + \psi_2^*.$$

where

$$\psi_1^+ \equiv L_x \int_{-h_1}^{0} \bar{v}dz, \quad \psi_1^* \equiv L_x\overline{v_1' h_1'}, \tag{7}$$

$$\psi_2^+ \equiv L_x \int_{-h_2}^{0} \bar{v}dz, \quad \text{and} \quad \psi_2^* \equiv L_x\overline{v_2' h_2'}.$$

Here, the overbar means zonal average, primes represent deviations from zonal average, ψ^+ represent the Eulerian-mean overturning circulation, ψ^* represents the eddy-driven overturning circulation, v is meridional velocity, h denotes pycnocline depth, $\psi = \psi^+ + \psi^*$ represents the residual-mean overturning circulation streamfunction associated with the two pycnoclines, and L_x is the longitudinal width of the Southern Ocean. The subscripts 1 and 2 indicate the layer each variable refers to (see Fig. 4). Physically, ψ_1 and ψ_2 represent the net meridional volume transport above the upper and lower pycnoclines, respectively. Because the bottom layer is assumed to be motionless and we also assume the circulation to be adiabatic below the surface mixed layer, we should obtain

$$\psi_1 = \Psi, \tag{8}$$

$$\text{and} \quad \psi_2 = 0,$$

where Ψ is a constant that defines the intensity of the AMOC and represents the effects of North Atlantic surface buoyancy conditions in our conceptual model.

In the Southern Ocean, the Eulerian zonal-mean momentum balance in steady state within the reentrant Southern Ocean is

$$-f_0\bar{v} = \frac{\partial F}{\partial z}, \text{ with } F = \frac{\tau_0}{\rho_0} \text{ at } z = 0, \tag{9}$$

where the nonlinear Reynolds terms and horizontal frictional forces have been neglected (Marshall and Radko, 2003), F represents vertical momentum flux, and τ_0 represents surface wind stress. For analytical simplicity, τ_0 and f_0 are assumed to be constant. The pressure gradient force is not present due to the absence of meridional boundaries in the Southern Ocean. The

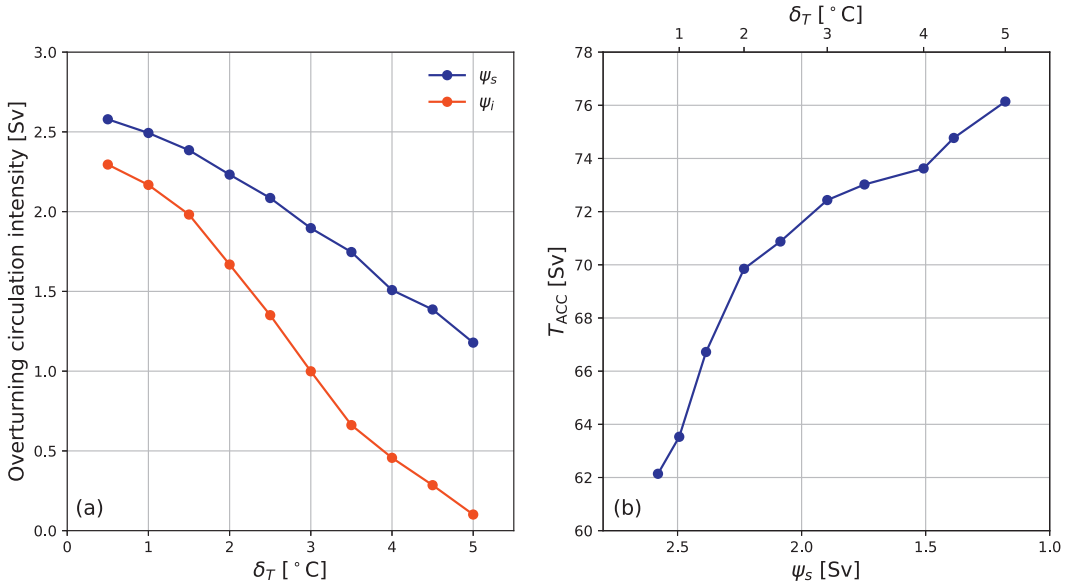

Fig. 3. (a) Variation of the magnitude of the AMOC (ψ_i) and Southern Ocean overturning circulation (ψ_s) with changes in δ_T. (b) Variation of the ACC transport T_{ACC} with respect to the decrease of ψ_s. The x-axis is reversed because ψ_s decreases with δ_T.

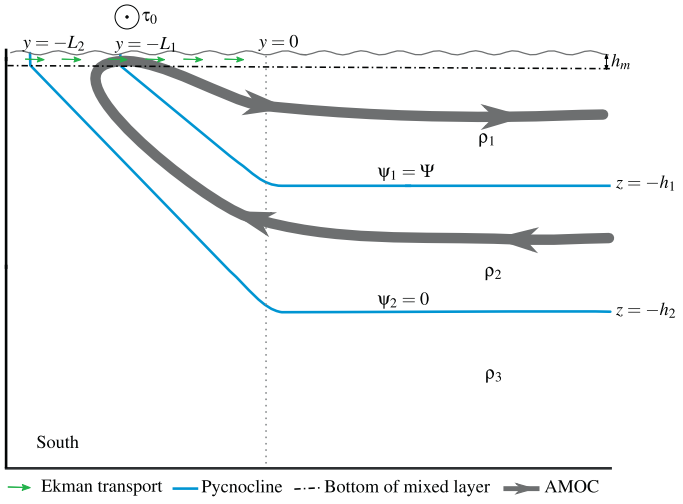

Fig. 4. Schematic of the 2.5-layer model. A mixed layer (dash–dotted line) of depth h_m is included that carries the Ekman transport (green arrow) in the Southern Ocean. The density of the three layers are ρ_1, ρ_2, and ρ_3 from top to bottom. The three layers are separated by two pycnoclines that are indicated as blue lines. The two pycnoclines outcrop at surface in the Southern Ocean at $y=-L_1$ and $y=-L_2$, respectively. The depth of the two pycnoclines are $z=-h_1$ and $z=-h_2$, respectively. The northern boundary of the Southern Ocean is represented by the gray dotted line ($y=0$). The thin gray sinusoidal line indicates the sea surface. The solid black line represents the bottom topography and the idealized Antarctica continent. The AMOC is carried by the top two layers and are represented by the thick gray lines with arrows indicating the directions of the overturning circulation. The streamfunction for the top pycnocline is noted as ψ_1, and the streamfunction for the bottom pycocline is noted as ψ_2. Only the southern hemisphere is plotted here. (For interpretation of the references to color in this figure legend, the reader is referred to the web version of this article.)

balance in Eq. (9) is valid as long as it is above the submarine sill. Vertical integration of Eq. (9) gives the expression of the Eulerian-mean overturning circulation streamfunction (ψ^+)

$$\psi^+|_z = L_x \int_z^0 \bar{v} dz = -\frac{\tau_0 L_x}{\rho_0 f_0}, \text{ for } -h_m > z > -h_s, \tag{10}$$

if the vertical momentum flux below the surface mixed layer is also neglected. Here, h_s is the depth of the submarine sill at the Drake passage, and h_m is the depth of surface mixed layer. Therefore, we can express ψ_1^+ and ψ_2^+ as

$$\psi_1^+ = \psi_2^+ = -\frac{\tau_0 L_x}{\rho_0 f_0}, \tag{11}$$

i.e., the Eulerian-mean overturning circulation streamfunction is given by the surface Ekman transport that is driven by the westerly wind over the Southern Ocean.

Following Gnanadesikan (1999), we can parameterize the eddy-driven overturning circulation (ψ_1^* and ψ_2^*) in Eq. (7) as

$$\begin{aligned} &\psi_1^* = L_x K_{\text{GM}} s_1, \\ \text{and} \quad &\psi_2^* = L_x K_{\text{GM}} s_2, \end{aligned} \tag{12}$$

where s_1 and s_2 are respectively the slope of the upper and lower pycnocline, and K_{GM} is the GM thickness diffusivity, which is assumed to be constant in this section. This assumption (constant K_{GM}) is relaxed in Section 4.2, where we discuss the potential influence of a more realistic representation of K_{GM} on the results.

Combining Eqs. (6), (8), (11), and (12), we have the expression for the residual-mean overturning circulation associated with the two pycnoclines

$$\begin{aligned} &\psi_1 = -\frac{\tau_0 L_x}{\rho_0 f_0} + L_x K_{\text{GM}} s_1 = \Psi, \\ \text{and} \quad &\psi_2 = -\frac{\tau_0 L_x}{\rho_0 f_0} + L_x K_{\text{GM}} s_2 = 0. \end{aligned} \tag{13}$$

From Eq. (13), we obtain the expression for the slope of the two pycnoclines as

$$\begin{aligned} &s_1(\Psi) = s_2 + \frac{\Psi}{L_x K_{\text{GM}}}, \\ \text{and} \quad &s_2 = \frac{\tau_0}{\rho_0 f_0 K_{\text{GM}}}. \end{aligned} \tag{14}$$

The parentheses in $s_1(\Psi)$ means that s_1 is subject to changes with respect to variations in Ψ. Because we keep the wind stress forcing (τ_0) and eddy effect (K_{GM}) constant, s_2 is also constant here. This implies an invariant depth of the lower pycnocline (h_2), i.e., h_2 is constant with respect to Ψ (Fig. 4), which is relaxed in the continuously stratified model in the next section.

From thermal wind balance, the zonal velocity at each layer can be expressed as

$$u_1 = u_2 - \frac{g_1'}{f_0}\frac{\partial h_1(\Psi)}{\partial y}, \tag{15}$$

and $u_2 = -\frac{g_2'}{f_0}\frac{\partial h_2}{\partial y}$,

where

$$h_1(\Psi) = -L_1 s_1(\Psi) \quad \text{and} \quad h_2 = -L_2 s_2. \tag{16}$$

Integrating Eq. (15) with respect to latitude and depth, we have the circumpolar transport of the ACC as

$$\begin{aligned} T_{\mathrm{ACC}}(\Psi) &= \int_{-L_s}^{0}\left[\int_{-h_2}^{-h_1} u_2 dz + \int_{-h_1}^{0} u_1 dz\right] dy \\ &= -\frac{1}{2f_0}\left[g_1' h_1^2(\Psi) + g_2' h_2^2\right]. \end{aligned} \tag{17}$$

To obtain sEq. (16) and (17), the assumption of $h_m \ll h_1$ is used. This assumption is true in both simulations and the real ocean. For example in the real ocean, h_m is normally of order 100 m, but h_1 is at around 1000 m. Because h_2 is constant here, changes in T_{ACC} can only be caused by variations in h_1, i.e.,

$$\Delta T_{\mathrm{ACC}}(\Psi) \equiv T_{\mathrm{ACC}}(\Psi) - T_{\mathrm{ACC}}(0) \approx -\frac{1}{f_0} g_1' h_1(0)\Delta h_1(\Psi), \tag{18}$$

where the changes are evaluated with respect to $\Psi = 0$,

$$h_1(0) = -L_1 s_1(0) = -L_1 s_2, \tag{19}$$

and

$$\Delta h_1(\Psi) = h_1(\Psi) - h_1(0) = -L_1[s_1(\Psi) - s_1(0)] = -\frac{L_1\,\Psi}{L_x K_{\mathrm{GM}}}, \tag{20}$$

which is obtained by combining Eq. (14) and Eq. (16).

Hereafter, the parentheses in $h(0)$ and $\Delta h(\Psi)$ will be dropped for conciseness. Dividing Eq. (18) by $T_{\mathrm{ACC}}(0)$, we have

$$\frac{\Delta T_{\mathrm{ACC}}(\Psi)}{T_{\mathrm{ACC}}(0)} \approx \frac{2g_1' h_1\,\Delta h_1}{g_1' h_1^2 + g_2' h_2^2} = \frac{2h_1\,\Delta h_1}{h_1^2 + h_2^2/r_g}, \tag{21}$$

where $r_g \equiv g_1'/g_2'$ is usually larger than 1 and defines the vertical structure of ocean density stratification in our 2.5-layer model.

Substituting Eq. (20) into Eq. (21), we have

$$\frac{\Delta T_{\mathrm{ACC}}(\Psi)}{T_{\mathrm{ACC}}(0)} \approx -\frac{2h_1 L_1 \Psi/L_x}{K_{\mathrm{GM}}\left[h_1^2 + h_2^2/r_g\right]}. \tag{22}$$

Substituting L_1 from Eq. (19) into Eq. (22), we have

$$\frac{\Delta T_{\mathrm{ACC}}(\Psi)}{T_{\mathrm{ACC}}(0)} \approx \frac{2h_1^2\,\Psi\,\rho_0\,f_0}{\tau_0 L_x\left[h_1^2 + \frac{h_2^2}{r_g}\right]} = -\Re\,\Gamma, \tag{23}$$

where h_1 is evaluated at $\Psi = 0$,

$$\Re \equiv \frac{2}{1 + \frac{1}{r_g r_h^2}} \tag{24}$$

represents the sensitivity of the ACC transport to the intensity of overturning circulation, $r_h = h_1/h_2$ represents the vertical structure of the overturning circulation, and

$$\Gamma \equiv \Psi/\psi^+ \tag{25}$$

is the residual-mean overturning circulation streamfunction normalized by the wind-driven overturning circulation streamfunction that is defined in Eq. (11). The negative sign in Eq. (23) indicates that the ACC transport decreases for a stronger overturning circulation consistent with Fig. 3(b). The variable Γ is a simplified representation of the North Atlantic surface buoyancy forcing in our conceptual model. For a larger r_h, the upper pycnocline is deeper and the ACC transport is more sensitive to the changes in the overturning circulation intensity and thus is more sensitive to surface forcing in the North Atlantic.

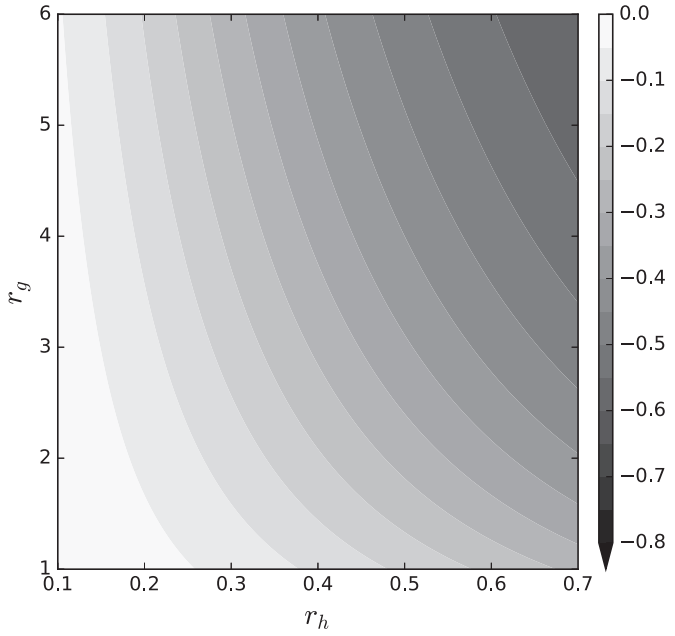

Fig. 5. Plot of $\Delta T_{\mathrm{ACC}}(\Psi)/T_{\mathrm{ACC}}(0)$ with respect to two nondimensional parameters r_g and r_h at $\Gamma = 0.4$. The nondimensional parameter r_g represents the shape of stratification, and r_h defines the structure of the overturning circulation. A larger r_g represents a stronger stratification in the mid-depth compared to the abyss. A larger r_h indicates that the overturning circulation has a deeper structure.

For parameters relevant to our MITgcm simulations at $\delta_T = 0.5\,^{\circ}\mathrm{C}$ in Section 2, $\Psi/L_x = 0.5\,\mathrm{m^2/s}$, $f_0 = 8\times10^{-5}\,\mathrm{s^{-1}}$, $\tau_0 = 0.1\,\mathrm{N/m^2}$, and $\rho_0 = 1000\,\mathrm{kg/m^3}$, the dependence of the relative change of circumpolar transport of the ACC ($\Delta T_{\mathrm{ACC}}/T_{\mathrm{ACC}}$) on these two non-dimensional parameters r_g and r_h is presented in Fig. 5. With slight change of the structure of the overturning circulation, the response of T_{ACC} to changes in the overturning circulation intensity can be substantially different. As an example, if we take $T_{\mathrm{ACC}}(0) = 100\,\mathrm{Sv}$, $r_g = 2.0$, and $\Psi/L_x = 0.5\,\mathrm{m^2/s}$ (corresponding to $\sim 10\,\mathrm{Sv}$ in the real ocean), $T_{\mathrm{ACC}}(\Psi)$ can be 81 Sv at $r_h = 0.4$ but is only 60 Sv at $r_h = 0.7$.

3.2. Continuous stratification

In the 2.5-layer conceptual model above, we use two pycnoclines to represent the upper overturning circulation cell. By warming the surface North Atlantic in our simulations, the overturning circulation structure is shifted to warmer temperatures (see Fig. 6). As a result, the depth associated with the zero-streamfunction (i.e., h_2 in our 2.5-layer model) becomes shallower as δ_T increases, although there is no significant change in the depth and potential temperature that is associated with the maximum overturning circulation streamfunction. This appears to account for the reduced sensitivity of the ACC transport to AMOC intensity for higher δ_T (Fig. 3(b)), which cannot be resolved by our simplified 2.5-layer conceptual model. Therefore, in order to make better comparison with our MITgcm simulations, we extend the 2.5-layer model to continuous stratification. Although the conceptual model below is presented in terms of density, we present our figures on potential temperature coordinate (e.g., Figs. 7 and 8) for better comparison with the MITgcm simulations.

In the Southern Ocean, we specify the surface density structure ($\rho_s(y)$) similar to the MITgcm simulations. The flow is assumed to be adiabatic again. With the surface wind stress forcing ($\tau(y)$) and the GM diffusivity (K_{GM}) specified, the residual-mean overturning circulation streamfunction ($\psi(\rho)$) in continuous stratification can be expressed as (Marshall and Radko, 2003; Nikurashin and Vallis, 2011)

$$\psi(\rho)/L_x = K_{GM}\, s(\rho, y) - \frac{\tau(y)}{\rho_0 f(y)}, \tag{26}$$

where both the wind stress forcing (τ) and isopycnal slope (s) vary with latitude. This is the continuously stratified version of Eq. (13). The isopycnal slope can be calculated from Eq. (26) as

$$s(\rho, y) = \left[\phi(\rho) + \frac{\tau(y)}{\rho_0 f(y)}\right]/K_{GM}, \tag{27}$$

where $\phi(\rho) = \Psi(\rho)/L_x$. Then the depth of each isopycnal can be found by integrating Eq. (27) as

$$z(\rho, y) = \int_{y_s(\rho)}^{y} s(\rho, y')dy' = \int_{y_s(\rho)}^{y} \left[\phi(\rho) + \frac{\tau(y')}{\rho_0 f(y')}\right]/K_{GM}dy', \tag{28}$$

which can be inverted to give the density structure $\rho(y, z)$ (see Figs. 5 and 6 of Marshall and Radko (2003) for examples). Here, $y_s(\rho)$ represents the outcropping latitude of each isopycnal (ρ) at the Southern Ocean surface. Applying the thermal wind balance by assuming the bottom to be motionless, we can calculate the ACC transport as

$$T_{ACC} = \int_{-L_s}^{0}\int_{-H}^{0}\int_{-H}^{z} \frac{g}{f(y)\rho_0}\frac{\partial \rho(y, z')}{\partial y} dz'\, dz\, dy, \tag{29}$$

where L_s is the meridional width of the reentrant channel, H is the depth of the ocean, and $-L_s \le y \le 0$ defines the range of the Southern Ocean as in Fig. 4. From Eqs. (28) and (29), we can see that the ACC transport is a function of only the residual-mean overturning circulation if we keep the wind stress forcing ($\tau(y)$) and eddy thickness diffusivity (K_{GM}) constant. The potential influence of wind stress forcing and eddy thickness diffusivity on the result is discussed in Section 4.1.

For simplicity, we adopt a form of surface density that linearly depends on y in the Southern Ocean, i.e.,

$$\rho_s(y) = -\Delta\rho\frac{y}{L_s} + \rho_r, \quad \text{for} \quad -L_s \le y \le 0, \tag{30}$$

where

$$\rho_s(0) = \rho_r, \tag{31}$$

and $\Delta\rho$ represents the density contrast across the Southern Ocean. The surface wind stress forcing is taken to be linear as well that resembles Fig. 1(b) in the Southern Ocean,

$$\tau(y) = \tau_0(y/L_s + 1), \quad \text{for} \quad -L_s \le y \le 0, \tag{32}$$

where

$$\tau_0 = 0.1\,\mathrm{N/m^2}. \tag{33}$$

The residual-mean overturning circulation streamfunction is assumed to be

$$\psi(\rho) = L_x\phi(\rho) = L_x\phi_0 M(\chi(\rho))\exp\left(-\lambda\xi(\rho)^2\right), \tag{34}$$

where

$$\xi(\rho) = \frac{\rho - \rho_d}{\rho_{l1} - \rho_{l2}}, \tag{35}$$

$$\chi(\rho) = \frac{\rho - \rho_{l2}}{\rho_{l1} - \rho_{l2}}, \tag{36}$$

and

$$M(\chi) = -\tanh(5(\chi - 1)) \times \tanh(5\chi) \tag{37}$$

for

$$\rho_{l1} \le \rho \le \rho_{l2}. \tag{38}$$

The function $M(\chi)$ is to ensure that ψ disappears for density outside of the density range defined by Eq. (38), and its form would not affect the result qualitatively. Here, $\rho_{l1} = \rho_s(0)$ is the lightest isopycnal associated with the overturning circulation, $\rho_{l2} = \rho_s(-L)$ is the densest isopycnal associated with the overturning circulation, ϕ_0 sets the magnitude of overturning circulation streamfunction, λ sets the spread of the streamfunction in density space (see Fig. 8(a) for examples),

$$\rho_d = \rho_{l1} + r_h^{\#}[\rho_{l2} - \rho_{l1}], \tag{39}$$

where $r_h^{\#}$ is a nondimensional number (similar to r_h in Section 3.1) that controls the position of maximum streamfunction in the density space (see Fig. 7(a) for examples). A larger λ means smaller spread of the overturning circulation in the density space (Fig. 8(a)), and a larger $r_h^{\#}$ means that the overturning circulation is associated with denser isopycnals (Fig. 7(a)). The two nondimensional parameters λ and $r_h^{\#}$ together control the vertical structure of the overturning circulation streamfunction in density space. We note that the forms of $\rho_s(y)$, τ_y, and $\psi(\rho)$ are chosen for illustrative purpose and will not affect our results qualitatively.

Consistent with the 2.5-layer conceptual model, we define the intensity of the overturning circulation (ϕ_m) as

$$\phi_m = \psi_m/L_x = \max\{\psi(\rho)\}/L_x, \text{ for } \quad \rho_{l1} \le \rho \le \rho_{l2}, \tag{40}$$

which represents the AMOC intensity and parameterizes the influence of the North Atlantic surface buoyancy condition on the overturning circulation intensity. Associated with the maximum streamfunction ψ_m, we also define a normalized AMOC intensity as

$$\Gamma_m = \psi_m/\psi^+, \tag{41}$$

where

$$\psi^+ = -\frac{\tau_0 L_x}{\rho_0 f_0}. \tag{42}$$

Now we explore the dependence of the ACC transport on the overturning circulation intensity (ϕ_m) and structure ($r_h^{\#}$) with constant wind stress forcing and eddy thickness diffusivity. In Fig. 7(b), we plot the relative changes in the ACC transport with respect to changes in both ϕ_m and $r_h^{\#}$. The relative change in T_{ACC} is defined as

$$R = \frac{T_{ACC}|_{\phi_m} - T_{ACC}|_{\phi_m=0}}{T_{ACC}|_{\phi_m=0}}, \tag{43}$$

where $T_{ACC}|_{\phi_m=0}$ represents the ACC transport at $\phi_m = 0$ and is a constant. This is similar to the definition in Eq. (21). Fig. 7(b) shows that variations of the ACC transport in response to changes in the overturning circulation intensity are strongly sensitive to the vertical structure of the overturning circulation, which is controlled by $r_h^{\#}$. For a larger $r_h^{\#}$, variations in ϕ_m are associated with changes in the overturning circulation on denser isopycnals, which means that changes in ϕ_m can affect the zonal-velocity distribution over a larger depth range and result in a bigger change in the ACC transport.

The sensitivity of the ACC transport can also be affected by λ, which sets the spread of streamfunction on density space. In Fig. 8(a), we plot the overturning circulation streamfunction for different λ to resemble the changes in the overturning circulation in Fig. 6. The response of the ACC transport to AMOC intensity changes is plotted in Fig. 8(b), in which the sensitivity of the

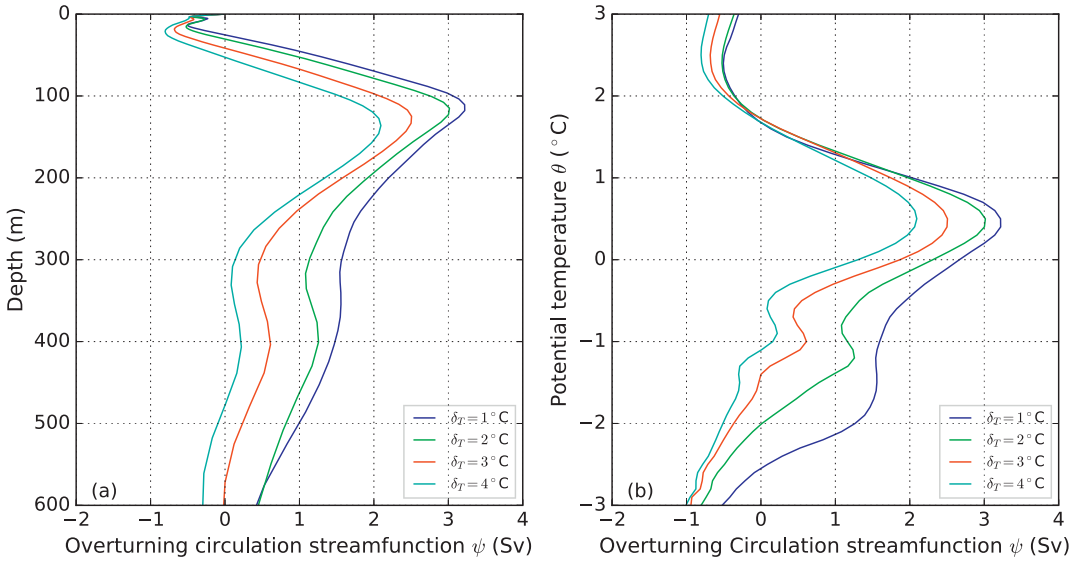

Fig. 6. Residual-mean overturning circulation at the northern edge of the reentrant Southern Ocean on depth coordinate (a) and θ coordinate (b). For clarity, only 4 runs are plotted.

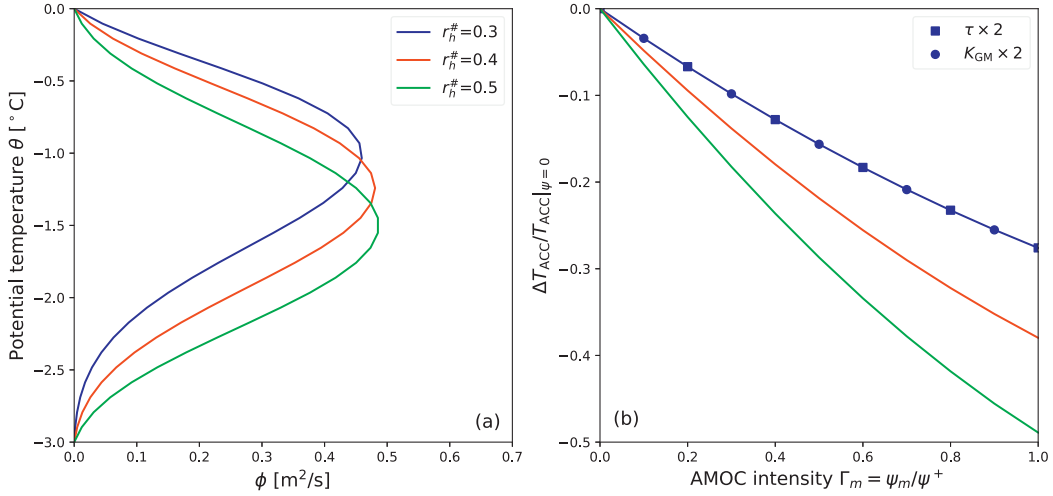

Fig. 7. (a) Residual-mean overturning circulation streamfunction defined by Eq. (34) for different $r_h^\#$ at $\phi_0 = 0.5$ and $\lambda = 10$. Larger $r_h^\#$ means that the overturning circulation is associated with higher density or lower potential temperature. The overturning circulation is only defined between $-3\,^\circ$C and $0\,^\circ$C here. The result would not change if a different potential temperature range is used. (b) Normalized changes in the ACC transport (normalized by the ACC transport at $\psi = 0$) with respect to changes in the normalized AMOC intensity (Eq. (42)) predicted by the continuously stratified conceptual model. Each line corresponds to a line in Panel (a) of the same color. The wind stress forcing and K_{GM} are doubled at $r_h^\# = 0.3$ and shown as blue squares and circles, respectively. This is discussed in Section 4.1. (For interpretation of the references to color in this figure legend, the reader is referred to the web version of this article.)

ACC transport to AMOC intensity is higher for smaller λ, which corresponds to a larger spread of the streamfunction in the density space. This explains the reduced sensitivity of the ACC transport in our MITgcm simulations for higher δ_T (compare Figs. 3(b) and6 with Fig. 8).

4. Discussion

4.1. Magnitude of wind stress forcing and K_{GM}

The 2.5-layer model in Section 3.1 (Eq. (23)) suggests that the response of the ACC transport to changes in the North Atlantic surface forcing is independent of the wind stress forcing (τ) and eddy thickness diffusivity (K_{GM}). We now test whether this is true in the continuously stratified conceptual model and the MITgcm simulations.

In the continuously stratified model, we double the wind stress forcing ($\tau \times 2$) and eddy thickness diffusivity ($K_{GM} \times 2$) but keep the overturning circulation structure (controlled by λ and $r_h^\#$) unchanged ($r_h^\# = 0.3$ in Fig. 7(a)). Although the intensity of the ACC and AMOC varies substantially in response to changes in the τ and K_{GM} (not shown), we find that the response of the normalized ACC transport to changes in the AMOC intensity is shown to be independent of the wind stress forcing and eddies (Fig. 7(b)), consistent with the 2.5-layer conceptual model.

However, this is not true in the MITgcm simulations because variations in the wind stress forcing and eddies could change the structure of the overturning circulation (e.g., Marshall et al., 2017). Using the same model setup as Section 2, another 3 sets of simulations are performed with increased wind stress forcing in the Southern Ocean. Each set of simulations contains 4 runs with $\delta_T = 1\,^\circ$C, $2\,^\circ$C, $3\,^\circ$C, and $4\,^\circ$C, respectively. We show that the sensitivity of the ACC transport to the AMOC intensity increases with

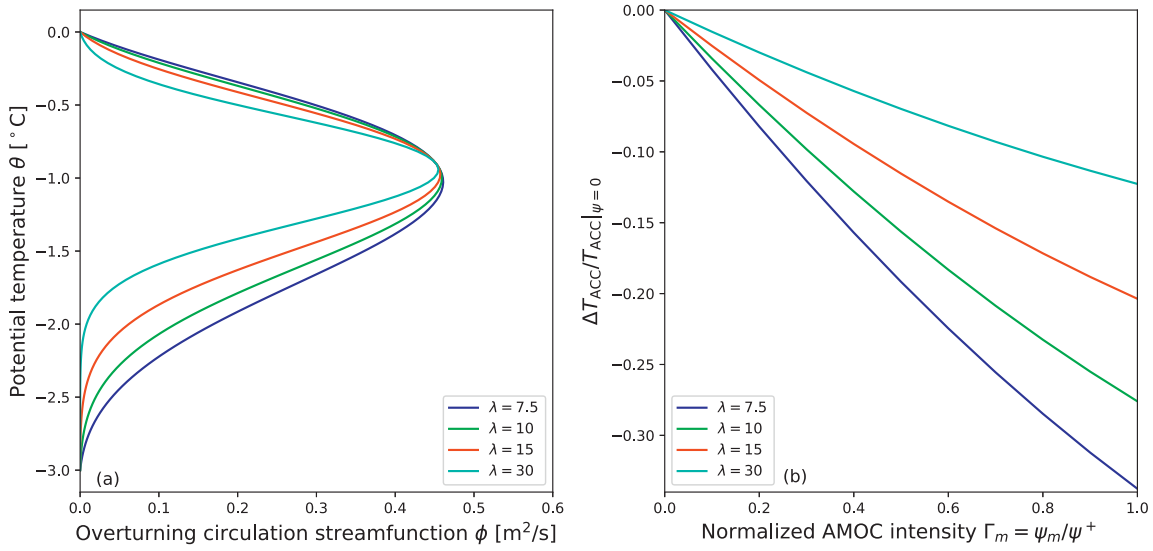

Fig. 8. (a) Residual-mean overturning circulation streamfunction defined by Eq. (34) for different λ at $\phi_0 = 0.5$ and $r_h^{\#} = 0.4$. This resembles the changes in the overturning circulation streamfunction in Fig. 6(b). Lower λ means that the overturning circulation is associated with more isotherms/isopycnals. (b) Normalized changes in the ACC transport with respect to the AMOC intensity normalized by the Eulerian-mean overturning circulation as predicted by the continuously stratified conceptual model. Each line corresponds to a line in Panel (a) of the same color.

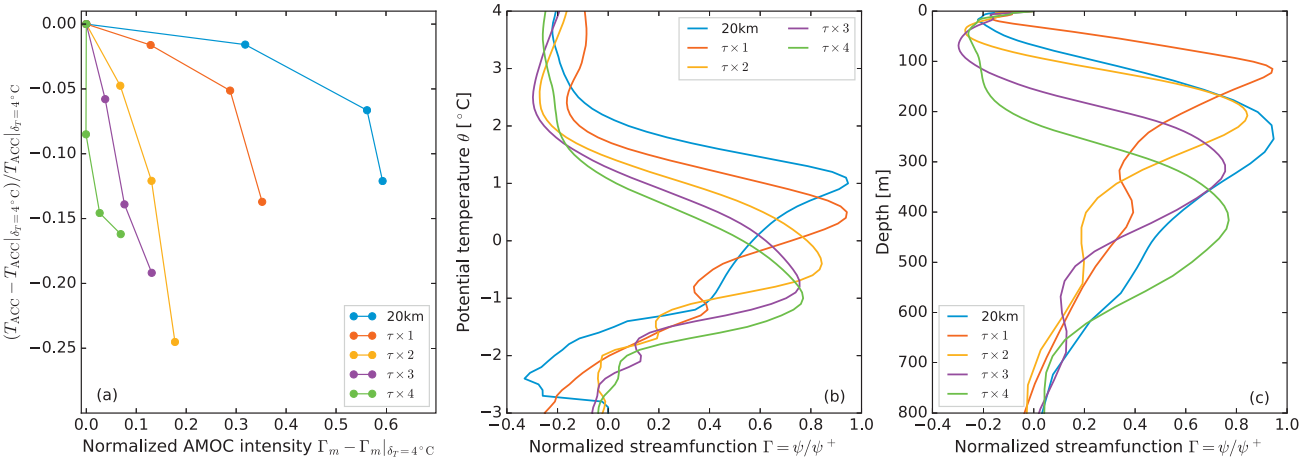

Fig. 9. (a) Variation of the ACC transport with the AMOC intensity at the northern edge of the Southern Ocean in the MITgcm simulations. The ACC transport is referenced to and then normalized by the ACC transport at $\delta_T = 4\,^\circ$C. The AMOC intensity is normalized by $\psi^+ = -\frac{\tau_0 L_x}{\rho_0 f_0}$, i.e., $\Gamma = \psi_s/\psi^+$, where ψ_s is defined in Eq. (5). From left to right, the four points in each set of simulation corresponds to $\delta_T = 4\,^\circ$C, $3\,^\circ$C, $2\,^\circ$C, and $1\,^\circ$C. Here, "$\tau \times n$" means that the wind stress forcing is multiplied by n in the Southern Ocean ("$\tau \times 1$" represents the simulations discussed in Section 2), and "20 km" refers to the simulation at 20 km resolution that is discussed in Section 4.3. (b) Normalized overturning circulation streamfunction at the northern edge of the reentrant Southern Ocean on θ coordinate at $\delta_T = 1\,^\circ$C. (c) Normalized overturning circulation streamfunction at the northern edge of the reentrant Southern Ocean on depth coordinate at $\delta_T = 1\,^\circ$C. The result is not significantly different for other choices of δ_T.

wind stress forcing (Fig. 9(a)) while the AMOC is shifted to colder potential temperature (Fig. 9(b)) and deeper depth (Fig. 9(c)) in the Southern Ocean, i.e., the overturning circulation structure changes with wind stress forcing. This increased sensitivity with wind can be reproduced by our continuously stratified conceptual model if the changes in the overturning circulation structure is considered such as by increasing $r_h^{\#}$ (Fig. 7).

We note that the conceptual models are developed just to interpret the influence of the AMOC structure on the ACC transport variations and thus should not be considered as complete models for the ACC or the overturning circulation in the Southern Ocean. To make a complete conceptual model, the influence of surface forcing on the intensity and structure of the overturning circulation needs to be parameterized. Therefore, in order to use our conceptual models to interpret model results, such as the different sensitivity at different wind stress forcing, the overturning circulation structure should be adjusted along with the model simulations such that they are dynamically in concert with each other.

4.2. State-dependent K_{GM}

In the conceptual model above, a constant GM thickness diffusivity is used. In this section, we relax this assumption and make it proportional to the isopycnal slope as suggested by Visbeck et al. (1997), i.e.,

$$K_{\mathrm{GM}} = k|s|, \tag{44}$$

where k is a positive scaling constant. As a result, the isopycnal slope in Eq. (14) becomes

$$s_2 = -\sqrt{\frac{\tau_0}{\rho_0 |f_0| k}}, \tag{45}$$

$$\text{and } s_1 = -\sqrt{s_2^2 - \frac{\Psi}{L_x k}}.$$

The change in h_1 with Ψ in Eq. (20) can be expressed as

$$\begin{aligned}\Delta h_1(\Psi) &= -L_1[s_1(\Psi) - s_2(0)] \\ &= \frac{h_1(0)}{s_2}\left[\sqrt{s_2^2} - \sqrt{\left(s_2^2 - \frac{\Psi}{L_x k}\right)}\right] \\ &= -h_1(0)\left[1 - \sqrt{(1-\Gamma)}\right],\end{aligned} \tag{46}$$

where Γ is the nondimensional residual-mean overturning circulation intensity that is defined in Eq. (25). Substitute Eq. (46) into Eq. (21) and we have

$$\frac{\Delta T_{\mathrm{ACC}}(\Psi)}{T_{\mathrm{ACC}}} \approx -\frac{-2h_1^2}{h_1^2 + h_2^2/r_g}\left[1 - \sqrt{(1-\Gamma)}\right], \tag{47}$$

where the parenthesis in $h_1(0)$ is dropped again for conciseness. For the upper overturning circulation cell discussed in this paper, $0 < \Gamma < 1$. Thus, we would obtain by Taylor expansion

$$\frac{\Delta T_{\mathrm{ACC}}(\Psi)}{T_{\mathrm{ACC}}} \approx -\frac{1}{2}\Re\Gamma, \tag{48}$$

where $\Re$ is defined in Eq. (24) and the terms of order $\mathcal{O}(\Gamma^2)$ and higher are dropped. Therefore, for a more realistic representation of K_{GM} that evolves with the model states, the sensitivity of the ACC transport to the overturning circulation is reduced by 50%. Similar results can be obtained for our continuously stratified conceptual model (not shown). This implies that the ACC sensitivity to the overturning circulation could also be reduced in OGCM simulations if the eddy is resolved or parameterized with a more realistic scheme (cf. Gent and Danabasoglu, 2011), as is also evidenced by the next section.

It is suggested by previous model studies that the eddy thickness diffusivity has a vertical structure that peaks at the top and bottom of the water column (e.g., Fig. 7 of Abernathey et al., 2013). This depth dependence of the eddy diffusivity is not resolved in our parameterization of the eddy thickness diffusivity, and it has been shown to have noticeable influences on the structure and magnitude of the overturning circulation (Chapman and Sallée, 2017). Future studies should employ more realistic representations of the eddy diffusivity. However, the discussion in this section suggests that a different parameterization of the eddy diffusivity would not change our results qualitatively.

4.3. Model resolution

Previous studies suggested that the ACC and the Southern Ocean overturning circulation can behave differently in response to surface forcing perturbations in models from coarse resolution to eddy-resolving resolution (e.g., Munday et al., 2013; Morrison and Hogg, 2013; Abernathey et al., 2011). Using an ocean basin similar to this study, Munday et al. (2013) showed that the ACC reaches eddy saturation when the model resolution is 1/2° and finer, consistent with Morrison and Hogg (2013). Here, the influence of model resolution on our results is tested with a set of experiments at 20 km resolution. The resolution of 20 km is chosen to represent the scenario with eddy saturation while it would not require too much computing resources.

In the 20 km resolution experiments, the GM thickness diffusivity is 20 m^2/s that represents an adiabatic sub-grid scale closure for the turbulent dissipation of potential temperature (cf. Munday et al., 2013; Roberts and Marshall, 1998). We also have a smaller biharmonic viscosity (A_4) of $1.0 \times 10^{12}\,\mathrm{m}^2/\mathrm{s}$ compared to the coarse-resolution simulations in Section 2 to damp the sub-grid noise close to the boundary and a small harmonic viscosity (A_h) of $2.0 \times 10^2\,\mathrm{m}^2/\mathrm{s}$ (cf. Griffies and Hallberg, 2000). The other parameters and model geometry follow the coarse-resolution model setup.

The model is spun up from rest and run for 500 years at $\delta_T = 1\,^\circ\mathrm{C}$. At the end of the 500 years, another three experiments are branched out with δ_T as 2 °C, 3 °C, and 4 °C. These four experiments are continued for another 500 years. Because eddies are permitted at this resolution that could enhance the Southern Ocean ventilation (e.g. Kamenkovich et al., 2017), it takes shorter time for the deep ocean to reach equilibrium (cf. Wolfe and Cessi, 2011). At the end of each simulation, the trend of ACC transport is less than 1 Sv/Century.

Different from the coarse-resolution runs, in which the changes in potential temperature space are consistent with changes in the depth space when the wind stress forcing increases, the overturning circulation in the 20 km-resolution simulations is shifted to warmer isotherms but deeper depth (Fig. 9). This discrepancy is due to the much smaller meridional temperature gradient in the Southern Ocean in the 20 km-resolution simulations (the temperature contrast across the Southern Ocean is reduced by 1 °C; not shown), which results from the higher eddy activity that enhances meridional heat flux across the ACC.

In the continuously stratified conceptual model, a fixed surface density structure is assumed at the Southern Ocean surface, which is not true when comparing the 20 km-resolution simulations to the coarse resolution runs. Therefore, the overturning circulation in depth space is a better indicator than that in the potential temperature space for comparing sensitivity of the ACC to the AMOC intensity here. Fig. 9(c) implies that the sensitivity of the ACC transport is at least larger than the simulation in Section 2 ("$\tau \times 1$" in Fig. 9) because the overturning circulation is located at a deeper depth. However, the sensitivity in the 20 km-resolution simulations is significantly smaller than expected (Fig. 9(a)). This is due to the higher eddy activity in the 20 km-resolution simulations that is more efficient in compensating the changes in the overturning circulation. Thus, a smaller change in the isopycnal slope is expected for increasing δ_T at this resolution compared to the coarse ones, consistent with what is concluded from the conceptual models that use a state-dependent eddy thickness diffusivity (Section 4.2). This implies that the sensitivity of the ACC to the surface conditions in the North Atlantic could be even smaller if the eddy is fully resolved.

5. Summary

The sensitivity of the circumpolar transport of the ACC to the North Atlantic surface buoyancy conditions is explored in a sector configuration of an ocean general circulation model. Because a fast restoring buoyancy boundary condition, which strongly constrains the surface buoyancy structure at the Southern Ocean surface, is used in this study, the ACC transport is determined by the isopycnal slope that is coupled to the overturning circulation. By changing the surface buoyancy in the North Atlantic, the shared buoyancy contour between the North Atlantic and the Southern Ocean is varied, and consequently the strength of the overturning circulation is modified. We find that the sensitivity in our simulations is substantially weaker than previous study by Fučkar and Vallis (2007). We propose that the different sensitivity relies on the different vertical structure of the simulated AMOC. For different depth of the simulated overturning circulation, the response of the ACC transport to changes in the strength of the overturning circulation varies substantially.

The results are interpreted using a 2.5-layer conceptual model and a continuously stratified conceptual model based on the residual-mean theory of the overturning circulation (Marshall and Radko, 2003). We show that the sensitivity depends on the vertical structure of the overturning circulation. Conceptually, this is true because a deeper change in the overturning circulation can affect more isopycnals by changing their slope, which leads to larger

changes in the circumpolar transport of the ACC. The wind stress forcing and eddies can affect this sensitivity by modifying the structure of the overturning circulation.

Considering that the structure of the overturning circulation varies substantially among different climate models especially in simulations of the LGM (e.g., Otto-Bliesner et al., 2007; Muglia and Schmittner, 2015), the sensitivity of the ACC transport is expected to vary significantly among different climate models. This has implication for discussions regarding the response of the ACC in simulations of the future climate change or paleo-climate variations.

The above analyses are based on coarse resolution model simulations, in which the mesoscale eddies are parameterized. We test the influence of model resolutions on the result by performing a set of eddy-permitting simulations and find that the sensitivity is smaller due to the higher eddy activity at this resolution. This implies that the sensitivity of the ACC transport to North Atlantic surface forcing is likely to be low in the real world, considering that the influence of the North Atlantic surface forcing on the ACC transport relies on changes in the isopycnal slope, which has been shown to be rather insensitive to external forcing perturbations in both observations (Böning et al., 2008) and model simulations (Gent and Danabasoglu, 2011).

In this study, we have focused on the upper overturning circulation cell that is assumed to be separated from the lower AABW overturning circulation cell. However, in the real ocean, the two overturning circulation cells are coupled to each other, forming a complex three-dimensional structure of the global overturning circulation (Talley, 2013). It is possible that the North Atlantic surface condition could impose a larger influence on the ACC through changes in the AABW overturning circulation, which has been shown to be able to significantly impact the ACC transport (Gent et al., 2001), than what is concluded in this paper. Future studies should address this by running a more complex model that resolves the three-dimensional structure of the overturning circulation.

Acknowledgments

This work used the Extreme Science and Engineering Discovery Environment (XSEDE), which is supported by National Science Foundation grant number ACI-1548562. S. Sun is supported by National Science Foundation grant OCE-1357078. Without implying their endorsement, the authors thank Ian Eisenman, Andrew Stewart, Ru Chen, Arjun Jagannathan, and Cesar Rocha for their helpful comments and discussions. The authors are also grateful for the helpful comments from two anonymous reviewers.

References

Abernathey, R., Ferreira, D., Klocker, A., 2013. Diagnostics of isopycnal mixing in a circumpolar channel. Ocean Model. 72, 1–16.
Abernathey, R., Marshall, J., Ferreira, D., 2011. The dependence of Southern Ocean meridional overturning on wind stress. J. Phys. Oceanogr. 41, 2261–2278.
Bishop, S.P., Gent, P.R., Bryan, F.O., Thompson, A.F., Long, M.C., Abernathey, R., 2016. Southern Ocean overturning compensation in an eddy-resolving climate simulation. J. Phys. Oceanogr. 46, 1575–1592.
Böning, C.W., Dispert, A., Visbeck, M., Rintoul, S., Schwarzkopf, F.U., 2008. The response of the antarctic circumpolar current to recent climate change. Nat. Geosci. 1, 864–869.
Chapman, C., Sallée, J.B., 2017. Isopycnal mixing suppression by the antarctic circumpolar current and the Southern Ocean meridional overturning circulation. J. Phys. Oceanogr 47, 2023–2045.
Downes, S.M., Hogg, A.M., 2013. Southern Ocean circulation and eddy compensation in AMIP5 models. J. Clim. 26, 7198–7220.
Ferrari, R., Griffies, S.M., Nurser, A.G., Vallis, G.K., 2010. A boundary-value problem for the parameterized mesoscale eddy transport. Ocean Model. 32, 143–156.
Ferrari, R., Jansen, M.F., Adkins, J.F., Burke, A., Stewart, A.L., Thompson, A.F., 2014. Antarctic sea ice control on ocean circulation in present and glacial climates. Proc. Natl. Acad. Sci. 111, 8753–8758.
Fučkar, N.S., Vallis, G.K., 2007. Interhemispheric influence of surface buoyancy conditions on a circumpolar current. Geophys. Res. Lett. 34, L14605.
Gent, P.R., 2016. Effects of southern hemisphere wind changes on the meridional overturning circulation in ocean models. Annu. Rev. Mar. Sci. 8, 79–84.
Gent, P.R., Danabasoglu, G., 2011. Response to increasing southern hemisphere winds in CCSM4. J. Clim. 24, 4992–4998.
Gent, P.R., Large, W.G., Bryan, F.O., 2001. What sets the mean transport through drake passage? J. Geophys. Res. Oceans 106, 2693–2712.
Gent, P.R., Mcwilliams, J.C., 1990. Isopycnal mixing in ocean circulation models. J. Phys. Oceanogr. 20, 150–155.
Gnanadesikan, A., 1999. A simple predictive model for the structure of the oceanic pycnocline. Science 283, 2077–2079.
Griffies, S.M., Hallberg, R.W., 2000. Biharmonic friction with a Smagorinsky-like viscosity for use in large-scale eddy-permitting ocean models. Mon. Weather Rev. 128, 2935–2946.
Haney, R.L., 1971. Surface thermal boundary condition for ocean circulation models. J. Phys. Oceanogr. 1, 241–248.
Hogg, A.M., 2010. An antarctic circumpolar current driven by surface buoyancy forcing. Geophys. Res. Lett. 37, L23601.
Ito, T., Woloszyn, M., Mazloff, M., 2010. Anthropogenic carbon dioxide transport in the Southern Ocean driven by Ekman flow. Nature 463, 80.
Jansen, M.F., Nadeau, L.P., 2016. The effect of Southern Ocean surface buoyancy loss on the deep ocean circulation and stratification. J. Phys. Oceanogr. 46, 3455–3470. doi:10.1175/JPO-D-16-0084.1.
Kamenkovich, I., Garraffo, Z., Pennel, R., Fine, R.A., 2017. Importance of mesoscale eddies and mean circulation in ventilation of the Southern Ocean. J. Geophys. Res. Oceans 122, 2724–2741.
Lamy, F., Arz, H.W., Kilian, R., Lange, C.B., Lembke-Jene, L., Wengler, M., Kaiser, J., Baeza-Urrea, O., Hall, I.R., Harada, N., et al., 2015. Glacial reduction and millennial-scale variations in drake passage throughflow. Proc. Natl. Acad. Sci. 112, 13496–13501.
Large, W.G., McWilliams, J.C., Doney, S.C., 1994. Oceanic vertical mixing: a review and a model with a nonlocal boundary layer parameterization. Rev. Geophys. 32, 363–403.
Lumpkin, R., Speer, K., 2007. Global ocean meridional overturning. J. Phys. Oceanogr. 37, 2550–2562.
Marshall, D.P., Zanna, L., 2014. A conceptual model of ocean heat uptake under climate change. J. Clim. 27, 8444–8465.
Marshall, J., Adcroft, A., Hill, C., Perelman, L., Heisey, C., 1997. A finite-volume, incompressible Navier Stokes model for studies of the ocean on parallel computers. J. Geophys. Res. Oceans 102, 5753–5766.
Marshall, J., Radko, T., 2003. Residual-mean solutions for the antarctic circumpolar current and its associated overturning circulation. J. Phys. Oceanogr. 33, 2341–2354.
Marshall, J., Scott, J.R., Romanou, A., Kelley, M., Leboissetier, A., 2017. The dependence of the ocean's MOC on mesoscale eddy diffusivities: a model study. Ocean Model. 111, 1–8.
Marshall, J., Speer, K., 2012. Closure of the meridional overturning circulation through Southern Ocean upwelling. Nat. Geosci. 5, 171–180.
Meijers, A., Shuckburgh, E., Bruneau, N., Sallee, J.B., Bracegirdle, T., Wang, Z., 2012. Representation of the antarctic circumpolar current in the CMIP5 climate models and future changes under warming scenarios. J. Geophys. Res. Oceans 117, C12008.
Morrison, A.K., Hogg, A.M., 2013. On the relationship between Southern Ocean overturning and ACC transport. J. Phys. Oceanogr. 43, 140–148.
Muglia, J., Schmittner, A., 2015. Glacial atlantic overturning increased by wind stress in climate models. Geophys. Res. Lett. 42, 9862–9868.
Munday, D., Allison, L., Johnson, H., Marshall, D., 2011. Remote forcing of the antarctic circumpolar current by diapycnal mixing. Geophys. Res. Lett. 38, L08609.
Munday, D.R., Johnson, H.L., Marshall, D.P., 2013. Eddy saturation of equilibrated circumpolar currents. J. Phys. Oceanogr. 43, 507–532.
Munk, W.H., Palmén, E., 1951. Note on the dynamics of the antarctic circumpolar current. Tellus 3, 53–55.
Nikurashin, M., Vallis, G., 2011. A theory of deep stratification and overturning circulation in the ocean. J. Phys. Oceanogr. 41, 485–502.
Nikurashin, M., Vallis, G., 2012. A theory of the interhemispheric meridional overturning circulation and associated stratification. J. Phys. Oceanogr. 42, 1652–1667.
Otto-Bliesner, B., Hewitt, C., Marchitto, T., Brady, E., Abe-Ouchi, A., Crucifix, M., Murakami, S., Weber, S., 2007. Last glacial maximum ocean thermohaline circulation: PMIP2 model intercomparisons and data constraints. Geophys. Res. Lett. 34, L12706.
Redi, M.H., 1982. Oceanic isopycnal mixing by coordinate rotation. J. Phys. Oceanogr. 12, 1154–1158.
Roberts, M., Marshall, D., 1998. Do we require adiabatic dissipation schemes in eddy-resolving ocean models? J. Phys. Oceanogr. 28, 2050–2063.
Sun, S., Eisenman, I., Stewart, A.L., 2016. The influence of Southern Ocean surface buoyancy forcing on glacial-interglacial changes in the global deep ocean stratification. Geophys. Res. Lett. 43, 8124–8132.
Talley, L.D., 2013. Closure of the global overturning circulation through the Indian, Pacific, and Southern Oceans: schematics and transports. Oceanography 26, 80–97.
Tamsitt, V., Talley, L.D., Mazloff, M.R., Cerovečki, I., 2016. Zonal variations in the Southern Ocean heat budget. J. Clim. 29, 6563–6579.
Toggweiler, J.R., Russell, J., 2008. Ocean circulation in a warming climate. Nature 451, 286–288.

Visbeck, M., Marshall, J., Haine, T., Spall, M., 1997. Specification of eddy transfer coefficients in coarse-resolution ocean circulation models. J. Phys. Oceanogr. 27, 381–402.

Wang, Z., Kuhlbrodt, T., Meredith, M.P., 2011. On the response of the antarctic circumpolar current transport to climate change in coupled climate models. J. Geophys. Res. Oceans 116, C08011.

Wolfe, C.L., Cessi, P., 2010. What sets the strength of the middepth stratification and overturning circulation in eddying ocean models? J. Phys. Oceanogr. 40, 1520–1538.

Wolfe, C.L., Cessi, P., 2011. The adiabatic pole-to-pole overturning circulation. J. Phys. Oceanogr. 41, 1795–1810.